The stripe critical point for cuprates

2000 J. Phys.: Condens. Matter 12 10655

(http://iopscience.iop.org/0953-8984/12/50/326)

J. Phys.: Condens. Matter **12** (2000) 10655–10666. Printed in the UK PII: S0953-8984(00)17351-5

The stripe critical point for cuprates

A Bianconi†, G Bianconi‡, S Caprara†, D Di Castro†, H Oyanagi§ and N L Saini†

† Unitá INFM and Dipartimento di Fisica, Università di Roma 'La Sapienza', 00185 Roma, Italy
‡ Department of Physics, Notre Dame University, IN-46566, USA
§ Electrotechnical Laboratory, 1-1-4 Umezono, Tsukuba 305-8568, Japan

E-mail: bianconi@superstripes.com

Received 21 September 2000, in final form 10 November 2000

Abstract. The experimental determination of the quantum critical point (QCP) that triggers the self-organization of charged striped domains in cuprate perovskites is reported. The phase diagram of doped cuprate superconductors is determined by a first variable, the hole doping δ, and a second variable, the micro-strain ε of the Cu–O bond length, obtained from the Cu K-edge extended x-ray absorption fine structure. For a fixed optimum doping, $\delta_c = 0.16$, we show the presence of the QCP for the onset of local lattice distortions and stripe formation at the critical micro-strain ε_c. The critical temperature $T_c(\varepsilon, \delta)$ reaches its maximum at the quantum critical point $(\varepsilon_c, \delta_c)$ for the formation of bubbles of superconducting stripes. The critical charge, orbital and spin fluctuations near this strain QCP provide the interaction for the pairing.

1. Introduction

The normal phase of cuprate superconductors shows the non-Fermi-liquid behaviour of a system close to a quantum critical point (QCP) [1–4]. Critical quantum fluctuations near a QCP drive the electron gas into a regime of strong interactions where the pairing mechanism for superconductivity is provided by a singular particle–particle interaction [6–10]. Therefore understanding the pairing mechanism for high-T_c superconductors (HTcS) requires the experimental determination of the quantum phase transition (QPT), with its QCP, for the cuprates. The QPT is a zero-temperature generically continuous transition tuned by a parameter in the Hamiltonian. Near this transition, quantum fluctuations take the system between two distinct ground states. The fluctuation between two nearly degenerate ground states is the characteristic feature of complex systems such as biological molecules [11]. In complex systems, the striped phases are a generic phenomenon where the one-dimensional ordering of the two ground states is driven by a long-range elastic, Coulomb or magnetic field.

The heterogeneous striped metallic phase in the cuprates where *'the free charges move mainly in one direction, like the water running in the grooves of a corrugated iron foil'* [12] is an expected feature of spatial self-organization near a QCP in complex systems. The stripe ordering in cuprates involves spin, charge and orbital degrees of freedom; therefore different experiments have indicated charge-density, orbital-density and spin-density waves (CDW, ODW and SDW) accompanied by local lattice fluctuations [13].

The properties of the normal phase of the cuprate perovskites have been assumed to depend on a single variable: the charge density measured by the doping δ, that gives the distance from the Mott–Hubbard antiferromagnetic phase. Several QPTs as functions of the doping have been

0953-8984/00/5010655+12$30.00

proposed and related to the curve $T_c(\delta)$ by various authors. However, it has not been possible to reach agreement on the location of the QCP at a critical doping since the experimental features indicating the quantum critical regime change from sample to sample.

Here we provide a solution showing that the QCP for the formation of superconducting stripes is on another relevant axis needed for the phase diagram of cuprates: the local strain ε of the average Cu–O bond length in the CuO_2 plane, called the micro-strain. By introducing this new axis we have measured the critical micro-strain ε_c for the onset of the striped phase, the two-dimensional (2D) phase diagram of the normal phase for all cuprate superconductors and the plot $T_c(\delta, \varepsilon)$, where the highest $T_c \sim 150$ K occurs at the QCP at $(\delta_c, \varepsilon_c)$.

The cuprate perovskites are heterogeneous materials [14] made of three different portions:

(i) *metallic bcc CuO_2 layers*;
(ii) *insulating rock-salt fcc AO_{1-x} layers* (A = Ba, Sr, La, Nd, Ca, Y); and
(iii) *charge-reservoir (CR) layers BO_{1-x}* where the chemical dopants are stored.

The superconducting bcc CuO_2 layer is intercalated between the insulating fcc rock-salt AO layers, rotated by 45°.

The mismatch between the two sublattices is $\eta = 1 - t = [R(\text{A–O})]/\sqrt{2}[R(\text{Cu–O})]$ where R(A–O) is the sum of the average metal-ion radius in the rock-salt layer r_A and the O^{2-} radius, R(Cu–O) is the Cu–O bond length and t is called the Goldschmidt tolerance factor. It is known that in hole-doped superconducting cuprates, the CuO_2 sheets are under compression due to the lattice mismatch. There are several experiments revealing the fact that the mismatch between the two sublattices produces a significant effect on the superconducting transition temperature [15–19]. The mismatch induces an anisotropic compressive stress on the CuO_2 plane that is different from the hydrostatic pressure [19].

The metallic phase in the CuO_2 plane is obtained by two separate steps:

- *first*, the doping δ in the CuO_2 plane is controlled by introducing the chemical dopants in the charge-reservoir blocks;
- *second*, the compressive stress on the CuO_2 plane is controlled by multiple substitutions of metal ions A (A = Ba, Sr, La, Nd, Ca, Y, ...) in the oxygen-deficient rock-salt (AO) layers. In fact, we found that the strain of the average Cu–O bond depends on the average ionic radius $\langle r_A \rangle$ of the rock-salt layers but not on the dopants in the charge-reservoir (BO) blocks.

In the materials where the dopants are introduced in the AO layers they act as impurity centres and form a disordered metallic phase, as is the case for Sr-doped La_2CuO_4.

There are now a growing number of experiments providing evidence for electron–lattice interaction being a necessary parameter for characterizing the metallic state of the cuprates [20–27]. Recent experiments on the isotope effects [28–30] have further indicated the need to include the electron–lattice interaction as one of the parameters for describing the complex metallic phase of the cuprate superconductors.

The doping δ shifts the system away from the Mott–Hubbard insulating phase and changes the ratio J/t of the antiferromagnetic coupling J to the single-electron hopping energy t. The compressive stress induces an elastic strain field ε in the CuO_2 plane that changes the electron–lattice coupling constant $g(\varepsilon)$. For example the pseudo-Jahn–Teller (JT) electron–phonon coupling [12, 20, 21], $g_{JT} = \Psi(Q, \beta, \Delta_{JT})$, depends on the conformational parameter for the local distortions of the CuO_4 square, Q, the rhombic distortion of the CuO_4 square plane, the dimpling angle β given by the displacement of the Cu ion from the plane of oxygen ions and the Cu–O (apical) bond length that controls the JT energy splitting Δ_{JT}. Therefore by changing the strain field the system can be driven toward charge localization.

The actual insulating phase in a doped magnetic insulator [31] depends on the charge density, i.e., doping δ; in fact for very low density we expect the formation of isolated polarons (and coexistence of polarons and free carriers in the intermediate-coupling regime [32]), while at higher density, strings [33] and charge-ordered phases [34] are expected; therefore the phase diagram of cuprates, beyond doping, requires as a second axis the micro-strain ε at the Cu site [13].

We have measured the micro-strain at the Cu site by exploiting the Cu K-edge extended x-ray absorption fine structure (EXAFS), which is a local and fast structural probe. From the average $\langle R_{\mathrm{Cu-O}} \rangle$ in the CuO_2 plane we have measured the micro-strain of the Cu–O bond defined as $\varepsilon = 2(d_0 - \langle R_{\mathrm{Cu-O}} \rangle)/d_0$ where the factor 2 is introduced to get the ratio $\varepsilon/\eta \sim 1$. Here d_0 is the Cu–O equilibrium distance, i.e., the Cu–O bond length for an unstrained CuO_2 plane. d_0 is measured to be $\sim$1.985($\pm$0.005) Å for an undoped model system $Sr_2CuO_2Cl_2$, which is consistent with other results [35]. d_0 is taken to be 1.97 Å throughout this paper, considering the effect of Cu–O shortening at optimum doping ($\delta \sim 0.16$ doped holes per Cu site). We have measured the local lattice fluctuations via the Debye–Waller factor of the Cu–O bond length as a function of the micro-strain. To avoid the disorder created by cationic substitution, we have selected the superconducting systems where the doping is provided only by the interstitial oxygen in the charge-reservoir blocks. The results provide direct experimental evidence for a large enhancement of the local lattice fluctuations at the critical micro-strain where the superconducting transition temperature T_c reaches its maximum.

2. Experimental procedure

Well-characterized superconducting single crystals of different superconducting systems were used for the experiments. The systems $La_2CuO_{4.1}$ (LCO), $Bi_2Sr_2CaCu_2O_{8+\delta}$ (Bi2212), $HgBa_2CuO_{4+\delta}$ (Hg1201) and $HgBa_2CaCu_2O_{6+\delta}$ (Hg1212)) systems are used as representative for the [BO](AO)CuO_2 heterostructures: $[O_\delta](La_2O_2)CuO_2$, $[Bi_2O_{2+\delta}](Sr_2O_2Ca)Cu_2O_4$, $[HgO_\delta](Ba_2O_2)CuO_2$ and $[HgO_\delta](Ba_2O_2Ca)Cu_2O_4$, where the (AO) rock-salt layers sustain different strain on the CuO_2 planes, and the dopants are interstitial oxygen ions in the charge-reservoir layers [BO]. An electrochemically doped LCO single crystal of size 2×2 mm^2 was used [36, 37]. This crystal has been characterized by x-ray diffraction showing 3.5 staging and a single $T_c \sim 40$ K ($\Delta T_c \sim 1.5$ K) measured before the experiments. The oxygen ordering of stage 3.5 occurs between 330 K to 270 K.

The Bi2212 crystal was of size 1×2 mm^2, grown by the travelling-solvent floating-zone method [38] with $T_c \sim 87$ K ($\Delta T_c \sim 1.2$ K). On the other hand, the Hg-based crystals were of small size ($\sim 0.3 \times 0.3$ mm^2), and were grown by a high-pressure synthesis technique [39]. The values of T_c for the samples used for the present experiments were 94 K ($\Delta T_c \sim 2$ K) and 116 K ($\Delta T_c \sim 3$ K) respectively for the Hg1201 and Hg1212.

The temperature-dependent polarized Cu K-edge absorption measurements were performed on the beam-line BL13B of the Photon Factory at the High Energy Accelerator Research Organization in Tsukuba and on the beam-lines BM29 and BM32 of the European Synchrotron Radiation Facility (ESRF), Grenoble. At the beam-line BL13B of the Photon Factory, and the beam-line BM32 of the ESRF, the crystals were mounted in a closed-cycle refrigerator and temperature was controlled within an accuracy of ± 1 K. The beam-line BM29 of ESRF is equipped with a two-stage closed-cycle refrigerator and the samples were mounted in it with temperature control within an accuracy of ± 1 K. In all cases, the temperature was measured using diode sensors attached to a flat-plate sample holder. The measurements were performed in the fluorescence-yield (FY) mode [40] using a multi-element Ge x-ray detector array. The emphasis was placed on measuring the spectra with a high signal-to-noise ratio

and up to a high momentum transfer, and we purposely measured several scans to accumulate the total fluorescence counts to ∼3 million to limit the relative errors to being less than 0.1% above the absorption threshold. The standard procedure was used to extract the EXAFS signal from the absorption spectrum and it was corrected for the x-ray fluorescence self-absorption before the analysis. Further details on the experiments and data analysis can be found in our earlier publications [27, 41–43].

3. Results and discussion

Figure 1 shows the Fourier transform (FT) of the EXAFS signals extracted from the Cu K-edge absorption spectra measured on different superconducting systems with the $\boldsymbol{E}$-vector of the plane-polarized x-ray beam falling parallel to the CuO_2 plane, representing different families. The inset shows the EXAFS oscillations (multiplied by k^2 to emphasize the higher k-region). The EXAFS oscillations are clearly visible up to the high k-values required to solve for quantitative local distortions in complex systems such as the high-T_c superconductors. The peaks in the FT are due to backscattering of photoelectrons, emitted at the Cu site, from neighbouring atoms providing a global atomic distribution around the absorbing Cu site. The peaks in the FT do not represent the real atomic distances and the position should be corrected for the photoelectron backscattering phase shifts to give a quantitative value to the atomic positions with respect to the Cu atom. There are evident differences between the FTs of the EXAFS spectra measured on different systems. The major difference appears around the Cu–A (A = La, Sr(Ca), Ba(Ca)) peak due to the different rock-salt layers.

The EXAFS amplitude depends on several factors as can be seen from the following EXAFS equation for polarized K-edge EXAFS [44]:

$$\chi(k) = \frac{m\pi}{h^2} \sum_i 3N_i \cos^2(\theta_i) \frac{S_0^2}{kR_i^2} f_i(k, R_i) \mathrm{e}^{-2R_i/\lambda} \mathrm{e}^{-2k^2\sigma_i^2} \sin[2kR_i + \delta_i(k)].$$

Here N_i is the equivalent number of neighbouring atoms, at a distance R_i, located at an angle θ_i with respect to the electric field vector of the polarized synchrotron light. S_0^2 is an amplitude correction factor due to photoelectron correlation (also called the passive electron reduction factor), $f_i(k, R_i)$ is the backscattering amplitude, δ_i are the phase shifts of the scattered photoelectrons, λ is the photoelectron mean free path and σ_i^2 is the correlated Debye–Waller factor of the photo-absorber–backscatterer pairs. The photoelectron wave-vector k is given by $E - E_0 = (\hbar k)^2/(2m)$ where E_0 defines the photoelectron energy origin. The phase shifts δ_i and E_0 can be either fixed or allowed to vary when an experimental EXAFS spectrum is parametrized.

Here we focus only on the local distortions in the CuO_2 plane and hence the first oxygen coordination shell (i.e. in-plane Cu–O bond distances). In the $\boldsymbol{E} \parallel \boldsymbol{a}$–$\boldsymbol{b}$ Cu K-edge EXAFS, the signal due to the Cu–O bond distances is well separated from the longer-bond contributions and can be easily extracted and analysed separately. The extracted EXAFS signals due to the Cu–O bond distances represent only single backscattering of the photoelectron emitted at the Cu site by its nearest-neighbour in-plane oxygen atoms and probe the correlation function of the Cu and oxygen pairs. The approach is designed to avoid any multiple-scattering signals that generally make the data analysis complex. We have used the standard procedures to draw the pair distribution function (PDF) of local Cu–O bond lengths from analysis of the EXAFS oscillations, just due to the Cu–O distances. In this procedure the EXAFS signal due to Cu–O is simulated by a standard least-squares fit with an input of distribution distances (where N_{tot} is fixed to the nominal value and σ^2_{CuO} for each distance is fixed to the value given by the Einstein model for correlated Cu–O distribution), restricting the number of allowed parameters to being

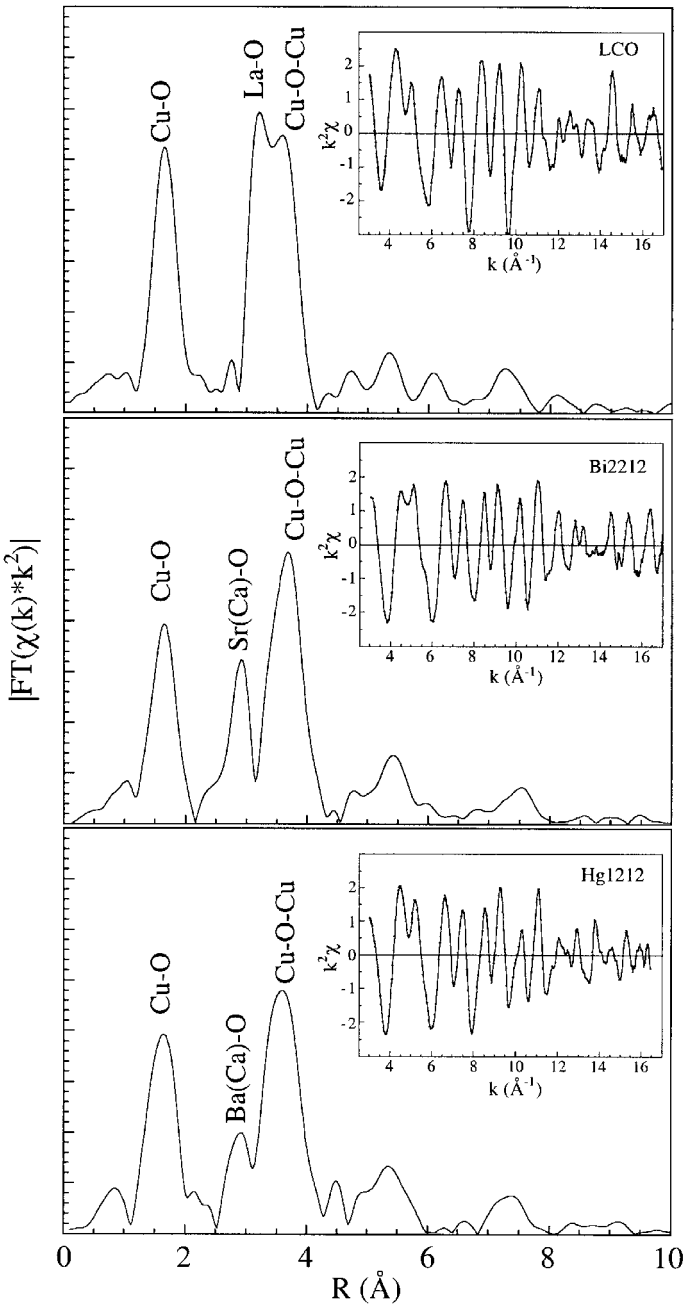

Figure 1. The Fourier transforms of the Cu K-edge EXAFS spectra of the representative systems measured in their superconducting states: LCO (upper), Bi2212 (middle), Hg1212 (lower). The insets show the corresponding EXAFS oscillations. The EXAFS signal was extracted from the absorption spectra measured for single-crystal samples using multi-element fluorescence detector systems in the $\boldsymbol{E} \parallel \boldsymbol{a}$–$\boldsymbol{b}$ geometry. The emphasis is placed on obtaining spectra with high signal-to-noise ratio, which is evident from the FT and the EXAFS oscillations up to high k-values.

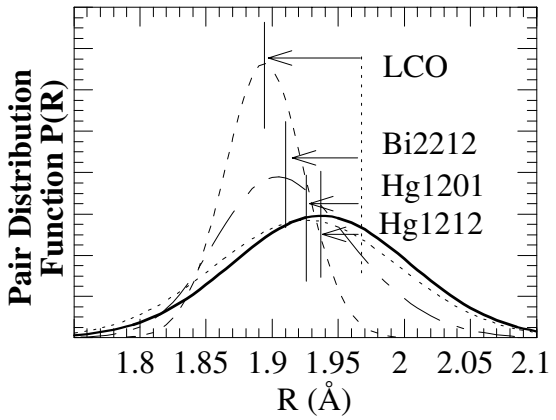

Figure 2. The Cu–O pair distribution function (PDF) in the normal state ($T = 200$ K) for different superconducting systems. The solid vertical bars refer to the mean Cu–O distances in the respective systems.

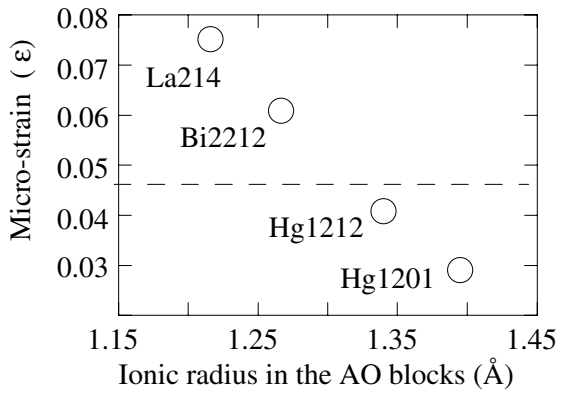

Figure 3. The micro-strain $\varepsilon = 2(d_0 - \langle R_{\mathrm{Cu-O}}\rangle)/d_0$, with $d_0 = 1.97$ Å obtained from the measure of the average $\langle R_{\mathrm{Cu-O}}\rangle$ bond length from Cu K-edge EXAFS is plotted as a function of the average radius $\langle r_{\mathrm{A}}\rangle$ of metal ions in the rock-salt layers.

less than $2\,\Delta R\,\Delta k/\pi$ [44]. The feasibility of these methods has been shown in the case of cuprates [27] and manganites [45] and other complex systems [46].

Figure 2 shows the Cu–O pair distribution function (PDF) in the LCO, Bi2212, Hg1201 and Hg1212 systems determined from the EXAFS spectra measured in the normal state ($T = 200$ K). The PDF represents the distribution of instantaneous Cu–O bonds. Above 200 K we observe a Gaussian distribution with a peak at the mean Cu–O distance $\langle R_{\mathrm{Cu-O}}\rangle$. The mean Cu–O bond lengths (vertical bars) show a clear evolution with the change in the stress due to the reduction of the average ionic radius r_{A} in the (AO) layers.

From the measure of $\langle R_{\mathrm{Cu-O}}\rangle$ we can obtain a direct measure of the micro-strain on the Cu–O bond $\varepsilon = 2(d_0 - \langle R_{\mathrm{Cu-O}}\rangle)/d_0$ (where $d_0 = 1.97$ Å is the equilibrium Cu–O distance at doping $\delta = 0.16$) in the different cuprate perovskites.

We report in figure 3 the variation of the micro-strain ε for the four samples reported on here (open circles) versus the average ionic radius in the rock-salt layers which is a measure of the lattice mismatch. The Cu–O bond lengths show a decrease, indicating an increasing

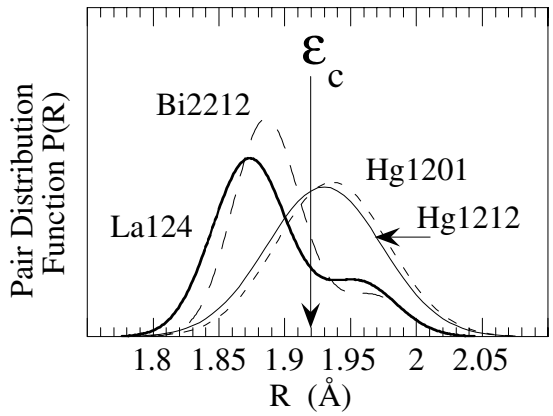

Figure 4. The Cu–O pair distribution function (PDF) at low temperature (in the superconducting state, $T \sim 0.5T_c$) for different superconducting systems. The systems where $\varepsilon > \varepsilon_c = 0.045$ show evidence for local lattice fluctuations with a PDF that does not have a Gaussian distribution but shows two peaks.

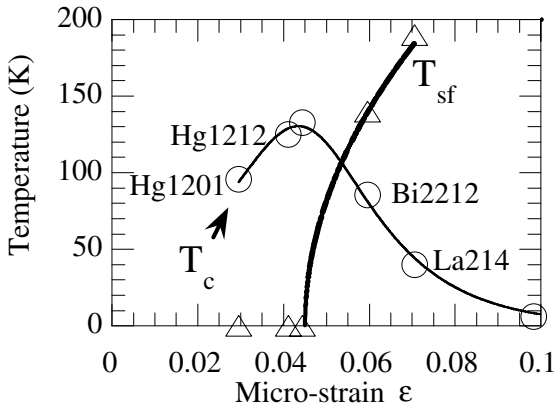

Figure 5. The critical temperature for charge ordering T_{sf} and the superconducting critical temperature T_c as functions of the micro-strain $\varepsilon = 2(d_0 - \langle R_{\mathrm{Cu-O}} \rangle)/d_0$ at optimum doping $\delta = 0.16$. We have added in this figure also two other samples studied by us: Hg1223 with maximum T_c near the critical strain and the 40% Nd-doped La2124 at very high micro-strain.

compressive strain of the Cu–O bond, with decreasing average ionic radius in the rock-salt layers. The structure is stable up to a value of the strain where the CuO_2 plane, or the rock-salt layer, or both, relax to a different structure that corresponds to a pressure of about 25 GPa [19].

In figure 4 we report the PDF for our crystals at fixed doping but at different micro-strains at $T < T_c$. We observe that, above a critical micro-strain $\varepsilon_c \sim 0.045$, the PDF shows the onset of local lattice distortions identified by the presence of two peaks in the PDF. We have determined the critical temperature for the formation of the local lattice distortion T_{sf} This temperature corresponds also to the critical temperature T_{sf} for the stripe formation as is shown by the onset of diffuse x-ray scattering peaks for LCO and Bi2212 at 190 K and 120 K respectively [37]. This charge ordering leads in Bi2221, where $\varepsilon > \varepsilon_c$, to the suppression of the spectral weight at the M point on the Fermi surface [48].

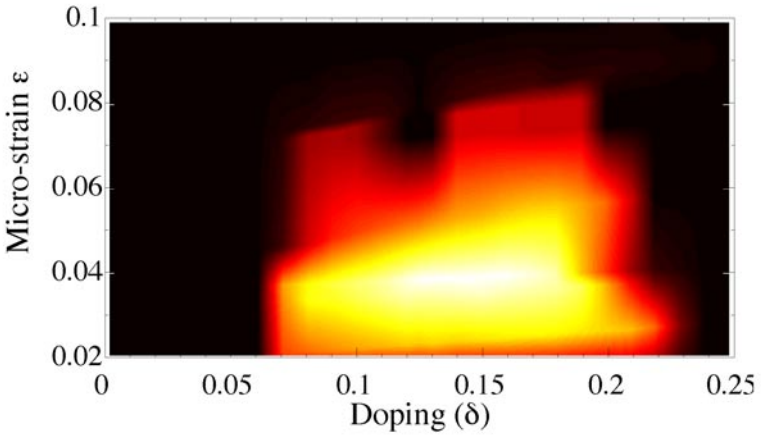

Figure 6. The superconducting critical temperature T_c plotted as a colour plot (from $T_c = 0$ K, black, to $T_c \sim 135$ K, through yellow to white) as a function of the micro-strain ε and doping δ. The maximum T_c occurs at the critical point $\delta_c = 0.16$, and $\varepsilon_c = 0.045$.

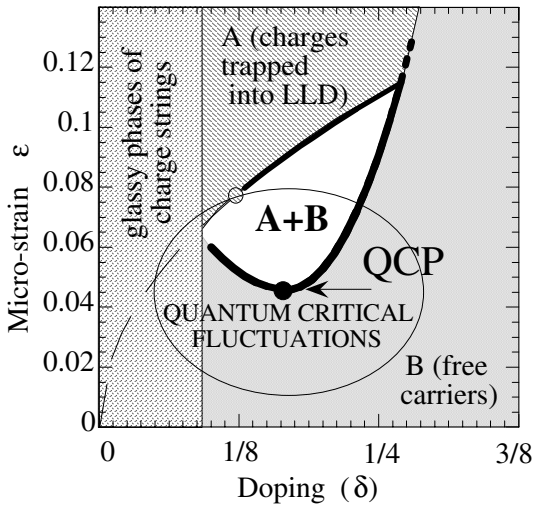

Figure 7. The phase diagram of the normal phase of doped cuprate perovskites as a function of micro-strain on the Cu–O(planar) bond and doping. The high-T_c superconductivity occurs in the region of quantum fluctuations around the micro-strain quantum critical point QCP.

We plot in figure 5 the value of the temperature for the onset of local lattice distortions and the 1D ordering of localized charge as a function of the micro-strain ε. The micro-strain ε drives the system to a QCP for the formation of a superlattice of quantum stripes for $\varepsilon > \varepsilon_c \sim 4.5\%$. In figure 6 we report the critical temperature T_c as a colour plot (the critical temperature increases from black, $T_c = 0$ K, through yellow to white, the maximum $T_c \sim 135$ K) as a function of the micro-strain ε and doping δ for all superconducting cuprate families. The figure shows that the maximum T_c occurs at the QCP ($\delta_c \sim 0.16$, $\varepsilon_c \sim 0.045$).

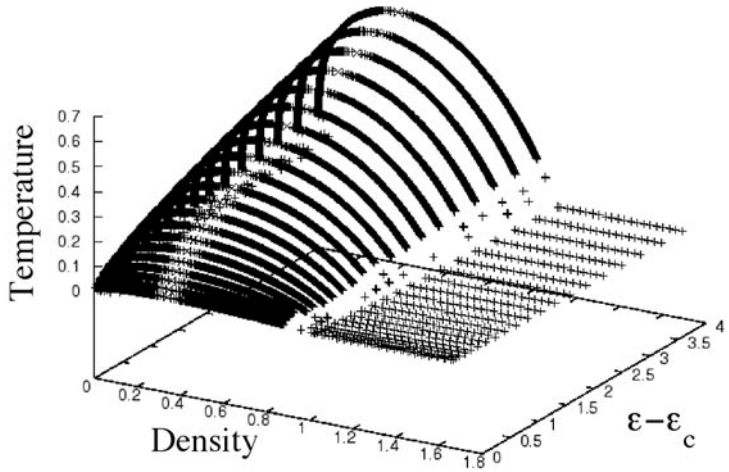

Figure 8. Phase-separation curves in the van der Waals scenario: temperature T versus density $(1/v$; i.e. the inverse of the specific volume) for different systems having different parameters a and b controlled by the micro-strain ε. The critical temperature goes to zero with $a \sim (\varepsilon - \varepsilon_c)^{1/2}$ and gives a QCP at ε_c as found from the experimental curve in figure 5.

From these data we can derive the qualitative phase diagram for the normal-metallic phase of all cuprate perovskites that give high-T_c superconductivity that is shown in figure 7. This phase diagram solves the long-standing puzzle of the phase diagram of the normal phase of the cuprates. There was a hidden physical parameter, the micro-strain, that triggers the electron–lattice interaction at a critical value for the onset of charges trapped into a striped phase with dynamical and spatial ordering of pseudo-Jahn–Teller local lattice distortions (JT-LLD). The doping of the strained antiferromagnetic lattice leads to the formation of both free carriers and charges trapped into the JT-LLD above the critical micro-strain ε_c. As has been shown for doped magnetic semiconductors, doped Mott–Hubbard insulators also show a phase-separation regime where metallic bubbles of doped charges are pushed away from the magnetic lattice. In the strong-electron–lattice-coupling regime, it has been shown for manganites that an inhomogeneous phase is formed by increasing the charge density as for a first-order phase transition [49]. It has been reported that cuprate perovskites (such as oxygen-doped Bi2212 and La124) that show slow stripe fluctuations for intermediate electron–lattice coupling, $\varepsilon > \varepsilon_c$, also show a quasi-first-order phase transition as a function of doping [50].

The QCP is well identified in the curve at constant doping as a function of the micro-strain ε, shown in figure 5. The simplest interpretation of figure 5 is that the QCP is at the end of a finite-temperature critical line for stripe formation $T_{sf}(\varepsilon)$. All the other transition points are first-order points which drive the system to a coexistence region (A + B). In this co-existence region fluctuating bubbles of superconducting stripes appear. These mesoscopic bubbles of about 100–300 Å with a short time scale are called 'superstripes'. In the phase diagram in figure 7 the superstripes appear (A+B) between the region A of the insulating charge ordered electron crystal and the region B of the homogeneous metal.

We can describe a scenario which is similar to the experimental one in the context of the van der Waals theory for real gases, which leads to the state equation

$$P = \frac{T}{v - b} - \frac{a}{v^2}$$

where P, T and v are pressure, temperature and specific volume. The parameter a measures the interparticle interaction while the parameter b is the hard-core specific volume. Different gases have different critical temperatures $T_{crit} = 8a/(27b)$; therefore the QCP would be reached for a tending to zero.

Figure 8 shows the temperature versus strain and density $(1/v)$ in the framework of the van der Waals scheme. The experimental results in figure 5 shown as T_{sf} versus strain correspond to the line of critical points parametrized by $a(\varepsilon)$. We have assumed $a = a_0(\varepsilon - \varepsilon_c)^{1/2}$ and $b = b_0 + b_1(\varepsilon - \varepsilon_c)$, where $b_0 = 1$, $a_0 = 1$ and $b_1 = 0.05$. The available experimental information does no exclude other possibilities, e.g., that there is a finite segment of quantum critical points around the QCP. Further experiments are under way to elucidate the orders of the various transition points.

In conclusion, we have shown a phase diagram for the superconducting phases where T_c depends on both doping and micro-strain. The plot $T_c(\varepsilon, \delta)$ reaches the highest temperature at the critical point $(\delta_c, \varepsilon_c)$. The anomalous normal phase of cuprate superconductors is determined by an inhomogeneous phase with coexisting polaronic stripes and itinerant carriers that appears for a local strain of the Cu–O bonds larger than a critical value. Fluctuations of orbital, charge and spin stripes appear in this critical regime of fluctuating mesoscopic bubbles of superconducting stripes called superstripes, that favour the amplification of the critical temperature.

Acknowledgments

The authors wish to acknowledge the ESRF scientific staff for experimental support. This research was supported by (i) the Ministero dell'Università e della Ricerca Scientifica (MURST) under the Programmi di Ricerca Scientifica di Rilevante Interesse Nazionale, (ii) Istituto Nazionale di Fisica della Materia (INFM) and (iii) Progetto 5% Superconduttività del Consiglio Nazionale delle Ricerche (CNR).

References

[1] Batlogg B and Varma C M 2000 *Phys. World* **13** (2) 33
[2] Sharma R P, Ogale S B, Zhang Z H, Liu J R, Chu W K, Veal B, Paulikas A, Zheng H and Venkatesan T 2000 *Nature* **404** 736
[3] Aeppli G, Manson T E, Hayden S M, Mook H A and Kulda J 1997 *Science* **278** 1432
[4] Valla T *et al* 1999 *Science* **285** 2110
[5] Sachdev S 1999 *Quantum Phase Transitions* (New York: Cambridge University Press)
[6] Millis A J, Monien H and Pines D 1990 *Phys. Rev.* B **42** 167
[7] Millis A J, Sachdev S and Varma C M 1988 *Phys. Rev.* B **37** 4975
[8] Bikers N E and White S R 1991 *Phys. Rev.* B **43** 8044
[9] Micnas R and Robaszkiewicz S 1992 *Phys. Rev.* B **45** 9900
Micnas R and Robaszkiewicz S 1995 *Phys. Rev.* B **52** 6863
[10] Perali A, Castellani C, Di Castro C and Grilli M 1996 *Phys. Rev.* B **54** 16 216
[11] Frauenfelder H Sligar S G and Wolynes P G 1991 *Science* **254** 1598
[12] Bianconi A 1993 *Phase Separation in Cuprate Superconductors* ed K A Müller and G Benedek (Singapore: World Scientific) pp 125, 352
Bianconi A and Missori M 1994 *J. Physique* I **4** 361

Bianconi A 1993 High T_c superconductors made by metal heterostructures at the atomic limit *European Patent* No 0733271 (priority date 7 December 1993; published in *Eur. Patent Bull.* 98/22, 27 May 1998)
Bianconi A, Valletta A, Perali A and Saini N L 1998 *Physica* C **296** 269
[13] Bianconi A, Agrestini S, Bianconi G, Di Castro D and Saini N L 2000 *Stripes and Related Phenomena* ed A Bianconi and N L Saini (New York: Kluwer/Plenum) p 9
Bianconi A, Di Castro D, Saini N L and Bianconi G 2000 *Proc. Cambridge Mtg (11–14 July 2000); Phase Transitions and Self-Organization in Electronic and Molecular Networks (Fundamental Materials Research Series)* ed M F Thorpe and J C Phillips (New York: Kluwer Academic/Plenum)
[14] Goodenough J B 1990 *Supercond. Sci. Technol.* **3** 26
Goodenough J B and Marthiram A 1990 *J. Solid State Chem.* **88** 115
Rao C N R and Ganguli A K 1995 *Chem. Soc. Rev.* **24** 1
[15] Attfield J P, Kharlanov A L and McAllister J A 1998 *Nature* **394** 157
[16] Locquet J P, Perret J, Fompeyrine J, Mächler E, Seo J W and Van Tendeloo G 1998 *Nature* **394** 453
[17] Ihara H 1994 *Bull. Electrotech. Lab.* **58** 64
Also see e.g. Izumi F and Takayama-Muromachi E 1995 *High Temperature Superconducting Materials and Engineering* ed D Shi (Oxford: Pergamon) p 81
[18] Sato H, Tsukada A, Naito M and Matsuda A 2000 *Phys. Rev.* B **61** 12 447
[19] Marezio M and Licci F 1997 *Physica* C **282** 53
[20] Seino Y, Kotani A and Bianconi A 1990 *J. Phys. Soc. Japan* **59** 815
[21] Bersuker G I and Goodenough J B 1997 *Physica* C **274** 267
[22] Zhou J-S and Goodenough J B 1997 *Phys. Rev.* B **56** 6288
[23] Müller K A, Zhao Guo-meng, Conder K and Keller H 1998 *J. Phys.: Condens. Matter* **10** L291
[24] Bozin E S, Billinge S J L, Kwei G H and Takagi H 1999 *Phys. Rev.* B **59** 4445
[25] McQueeney R J, Petrov Y, Egami T, Yethiraj M, Shirane G and Endoh Y 1999 *Phys. Rev. Lett.* **82** 628
[26] Sharma R P, Ogale S B, Zhang Z H, Liu J R, Wu W K, Veal B, Paulikas A, Zhang H and Venkatesan T 2000 *Nature* **404** 736
[27] Bianconi A, Saini N L, Lanzara A, Missori M, Rossetti T, Oyanagi H, Yamaguchi H, Oka K and Ito T 1996 *Phys. Rev. Lett.* **76** 3412
[28] Lanzara A, Zhao G-m, Saini N L, Bianconi A, Conder K, Keller H and Müller K A 1999 *J. Phys.: Condens. Matter* **11** L541
[29] Rubio Temprano D, Mesot J, Janssen S, Conder K, Furrer A, Mutka H and Müller K A 2000 *Phys. Rev. Lett.* **84** 1990
[30] Hofer J, Conder K, Sasagawa T, Zhao Guo-meng, Willemin M, Keller H and Kishio K 2000 *Phys. Rev. Lett.* **84** 4192 and references therein
[31] Nagaev E L 1972 *JEPT Lett.* **16** 558
[32] Cataudella V, De Filippis G and Iadonisi G 1999 *Phys. Rev.* B **60** 15 163
[33] Kusmartsev F V 2000 *Phys. Rev. Lett.* **84** 530
Kusmartsev F V 2000 *Phys. Rev. Lett.* **84** 5026
[34] Kusmartsev F V, Di Castro D, Bianconi G and Bianconi A 2000 *Phys. Lett.* A **275** 117
[35] Miller L L, Wang X L, Wang S X, Stassis C, Johnston D C, Faber J Jr and Loong C-K 1990 *Phys. Rev.* B **41** 1921
[36] Chou F C, Johnston D C, Cheong S W and Canfield P C 1993 *Physica* C **216** 66
[37] Bianconi A, Di Castro D, Bianconi G, Pifferi A, Saini N L, Chou F C, Johnston D C and Colapietro M 2000 *Physica* C **341–348** 1719
[38] Ha D H, Oka K, Iga F, Unoki H and Nishihara Y 1993 *Advances in Superconductivity V* ed Y Bando and H Yamauchi (Tokyo: Springer) p 323
[39] Karpinski J, Schwer H, Mangelschots I, Conder K, Morawski A, Lada T and Paszewin A 1994 *Physica* C **234** 10
[40] Oyanagi H, Shioda R, Kuwahara Y and Haga K 1995 *J. Synchrotron Radiat.* **2** 99
Oyanagi H 1998 *J. Synchrotron Radiat.* **5** 48
[41] Saini N L, Lanzara A, Oyanagi H, Yamaguchi H, Oka K, Ito T and Bianconi A 1997 *Phys. Rev.* B **55** 12 759
[42] Lanzara A, Saini N L, Bianconi A, Hazemann J L, Soldo Y, Chou F C and Johnston D C 1997 *Phys. Rev.* B **55** 9120
[43] Bianconi A, Saini N L, Lanzara A, Missori M, Rossetti T, Oyanagi H, Yamaguchi H, Oka K and Ito T 1996 *Phys. Rev. Lett.* **76** 3412
Saini N L, Lanzara A, Bianconi A and Oyanagi H 1998 *Phys. Rev.* B **58** 11 768
[44] Prinz R and Koningsberger D (ed) 1988 *X-Ray Absorption: Principle, Applications, Techniques of EXAFS, SEXAFS and XANES* (New York: Wiley)

[45] Lanzara A, Saini N L, Brunelli M, Natali F, Bianconi A, Radaelli P G and Cheong S-W 1998 *Phys. Rev. Lett.* **81** 878
[46] Stern E A, Ma Y, Hanske-Petitpierre O and Bouldin C E 1992 *Phys. Rev.* B **46** 687
[47] Babanov Y A and Shvetsov V R 1986 *J. Physique Coll.* **47** C8 37
Babanov Y A and Shvetsov V R 1986 *J. Non-Cryst. Solids* **79** 1
[48] Saini N L, Avila J, Bianconi A, Lanzara A, Asensio M C, Tajima S, Gu G D and Koshizuka N 1997 *Phys. Rev. Lett.* **79** 3467
[49] Nagaev E L, Podelshchikov A I and Zil'berwarg V E 1998 *J. Phys.: Condens. Matter* **10** 9823
Nagaev E L 1983 *Physics of Magnetic Semiconductors* (Moscow: Mir)
[50] Bianconi A 1994 *Physica* C **235–240** 269
Bianconi A 1994 *Sol. State Commun.* **91** 1